Available online at www.sciencedirect.com
SCIENCE DIRECT®
ELSEVIER
European Journal of Mechanics B/Fluids 25 (2006) 491–504
EUROPEAN JOURNAL OF MECHANICS B/FLUIDS

Electrically-excited (electroosmotic) flows in microchannels for mixing applications

Ingo Meisel [a], Peter Ehrhard [b,*]

[a] *Forschungszentrum Karlsruhe, Institute for Micro Process Engineering, P.O. Box 3640, 76021 Karlsruhe, Germany*
[b] *University of Dortmund, Biochemical & Chemical Engineering, Fluid Mechanics, Emil-Figge-Str. 68, 44221 Dortmund, Germany*

Received 17 January 2005; received in revised form 14 November 2005; accepted 10 December 2005

Available online 14 February 2006

Abstract

We propose an asymptotic model for quite general liquid microchannel flows in the presence of electrical double layers (EDLs). The model provides an "inner" solution for the wall layer, which reflects the dominant balance between electrical forces and viscous forces (tangentially), respectively between electrical forces and pressure and viscous forces (normally). The electrically-neutral core of the flow is governed by the standard Navier–Stokes equations, providing the "outer" solution. The asymptotic matching of both solutions provides a method for the simplified numerical treatment of such EDLs. The superposition of the solutions in both regions then allows to infer an approximate solution, valid within the entire domain.

Based on this model, we apply external oscillatory electrical fields to excite secondary flows (i) in microchannels with an internal obstacle or (ii) in folded (meander) microchannels. These secondary flows are demonstrated to greatly enhance the mixing of two liquids flowing in a layered fashion through these microchannels. Thus, electrical excitation has considerable potential if micromixers for ionic liquids are designed within electrically-insulating (e.g. plastics, glass) substrates.

Keywords: Microflow; Microchannel; Micromixer; Ionic liquids; Electrically-insulating solids; Electroosmosis; EDL; Electrical excitation; Secondary flow; FEM; Matched asymptotic solution

1. Introduction

Liquids are often characterized by the presence of positive and negative charges (ions). In contact with electrically non-conducting channel walls, the walls usually acquire a surface charge (cf. Hunter [1]). This surface charge at the wall attracts counter-ions from within the liquid, inducing a thin electrically non-neutral layer immediately at the wall. This layer is termed electrical double layer (EDL) (cf. Adamson and Gast [2]), whereas its thickness can be characterized by the Debye length l_D, which typically is much smaller than 1 μm. In contrast to the liquid in the EDL, the liquid in the channel core is not affected by the wall surface charges and remains electrically neutral. If electrical fields are present, either self-induced or externally applied, electrical forces act on the ions within the EDL, accelerating likewise surrounding liquid molecules by means of viscous drag. The resulting movement is known as

* Corresponding author.
E-mail address: p.ehrhard@bci.uni-dortmund.de (P. Ehrhard).

0997-7546/$ – see front matter
doi:10.1016/j.euromechflu.2005.12.002

electroosmotic flow (cf. Probstein [3]). In macroscopic flows electrical forces usually can be neglected against conventional forces resulting from pressure, inertia, viscosity or gravity. In microchannels, in contrast, forces at interfaces take a more prominent role due to the increasing ratio of interfacial area and volume with decreasing channel width (cf. Gad-el-Hak [4]). If electrical forces are then of similar magnitude to volumetric forces, they may be utilized to drive or modify the flow.

In the literature, electroosmotic flows, particularly in microchannels, have received considerable attention. Interest ranges from analytical solutions for fully-developed gap or pipe flows as a consequence of externally-applied fields, as e.g. given by Burgreen and Nakache [5] or Rice and Whitehead [6], to the fully-numerical treatment of such flows in more complex geometries, as e.g. reported by Patankar and Hu [7] or Kim et al. [8]. In all these articles the properties of the electrical double layer (EDL) are assumed constant. Recent work by Ghosal [9] even addresses the effect of slow variations of the channel cross section or the wall charge along the channel axis on the electroosmotic flow. One of the reasons for the sustained interest in electroosmotic flows lies in its wide range of applications in microfluidic devices as e.g. miniaturized total analysis systems (μTAS) (cf. Jakeway et al. [10]). Not only can electrical fields serve in such systems as an efficient method to transport liquids, moreover, they allow for the separation or focusing of differently-charged species by means of so-called electrophoretic effects.

Mixing in microchannels is considered to be a non-trivial task (cf. Jakeway et al. [10]). In general, efficient mixing of liquids can be viewed as a two-step process: (i) the "virtual interface" between the liquids to be mixed is increased in area, (ii) mass diffusion completes the mixing process on the molecular length scale (cf. Ottino [11]). Here "virtual" is used since mixing of miscible liquids is of interest. In contrast to macroscopic channel flows, the flow in microchannels often is characterized by small Reynolds numbers. Therefore, inertial effects are weak and cannot serve to increase the virtual interface through instabilities or even turbulence. Other means have to be applied in microchannels to achieve this increase of the virtual interface.

A number of methods have been proposed in literature for efficient mixing in microchannels. Passive methods include the split-up of the liquid streams into lamellae and subsequent recombination, so-called multilamination, as discussed e.g. by Hessel et al. [12] or Hardt and Schönfeld [13]. Further, complex three-dimensional serpentine channels are employed by e.g. Liu et al. [14] or Beebe et al. [15] to implement chaotic advection for enhanced mixing. Finally, relief structures embossed into the channel wall are utilized e.g. by Stroock et al. [16] to create secondary transverse flows in microchannels that can be used to induce chaotic stirring. All the above methods involve the manufacturing of more (or less) complex three-dimensional microchannels. Active methods, in contrast, often allow for simple channel geometry while some means of forcing needs to be introduced. Examples are the application of magnetohydrodynamic forces as discussed by Yi et al. [17]. These authors apply a uniform magnetic field in conjunction with steady or time-dependent electrical currents, driven between electrodes through the liquid, to induce chaotic advection capable to stir the liquid. Similar capabilities are identified by Qian and Bau [18] from electroosmotic forces. Here the interplay of a uniform electrical field and a time-dependent zeta potential is demonstrated to likewise induce chaotic advection. Another approach by Oddy et al. [19] engages electrokinetic forces to excite a channel flow. These authors apply time-dependent electrical fields to induce an "electrokinetic instability", which is demonstrated to fold and stretch the virtual interface, and thus appears promising for mixing.

The present article has its focus on liquid flows, excited by time-dependent electrical fields. In contrast to Oddy et al. [19], who excite the channel flow in wall-tangential direction to create unstable velocity profiles, we use an obstacle or a meander to introduce walls which are oriented perpendicular to the main flow direction. This allows acceleration of liquid along these walls by electrical forces and formation of streams which penetrate into the main flow. This method will be demonstrated to substantially improve mixing via the folding and stretching of the virtual interface.

The mathematical treatment of the electroosmotic flow in the present article differs from approaches adopted in previous work. Instead of either assuming electroosmotic slip at the solid walls or fully resolving the electrical double layer (EDL) numerically, we develop a matched-asymptotic treatment of the problem. This appears reasonable, since even in microchannels the thickness of the EDL (measured by l_D) usually is much smaller than the channel width d_0. Therefore, inferring solutions for two different regions, namely the wall layer and the channel core, appears to be a natural method. The matching and superposition of these solutions then results in an approximate solution, valid in the entire domain.

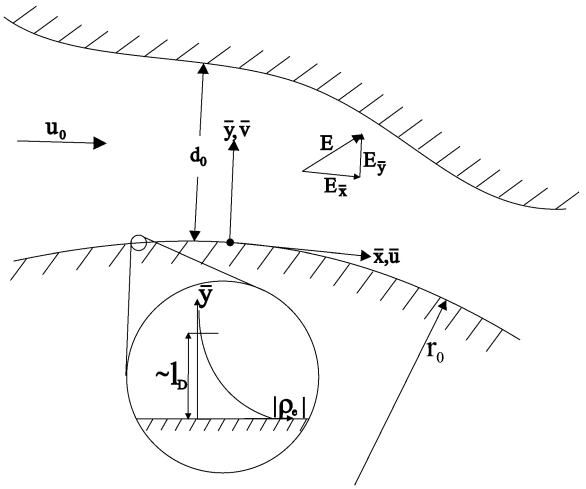

Fig. 1. Electrical double layer (EDL) in liquid flow in a microchannel of general geometry.

2. Mathematical formulation

2.1. Conservation equations

We focus on the plane problem of a channel of quite general geometry, a channel width of the order d_0 and a liquid velocity of the order u_0 (cf. Fig. 1). Although flows in roughly square microchannels will be three-dimensional in general, we employ a two-dimensional simulation to obtain a first approximation, valid in the mid plane of the channels. The time-dependent conservation equations for mass and momentum in presence of electrical forces read as

$$\frac{\partial u}{\partial x} + \frac{\partial v}{\partial y} = 0, \tag{1}$$

$$\rho\left(\frac{\partial u}{\partial t} + u\frac{\partial u}{\partial x} + v\frac{\partial u}{\partial y}\right) = -\frac{\partial p}{\partial x} + \mu\left(\frac{\partial^2 u}{\partial x^2} + \frac{\partial^2 u}{\partial y^2}\right) + \rho_e E_x, \tag{2}$$

$$\rho\left(\frac{\partial v}{\partial t} + u\frac{\partial v}{\partial x} + v\frac{\partial v}{\partial y}\right) = -\frac{\partial p}{\partial y} + \mu\left(\frac{\partial^2 v}{\partial x^2} + \frac{\partial^2 v}{\partial y^2}\right) + \rho_e E_y. \tag{3}$$

Within Eqs. (1)–(3) the Cartesian coordinates are denoted by (x, y), the velocity vector by $\mathbf{u} = (u, v)$, pressure by p, time by t, dynamic viscosity by μ, and density by ρ. Further, ρ_e is the (electrical) net charge distribution and $\mathbf{E} = (E_x, E_y)$ is the local electrical field vector.

2.2. Non-dimensional local equations

It is convenient to introduce a coordinate system $(\bar{x}, \bar{y})$ with the origin at the wall (cf. Fig. 1). Conceptually, the so-called Stern layer of immobile ions immediately at the wall belongs to the wall. Within such local tangential/normal coordinates the net charge distribution ρ_e within the electrical double layer (EDL) can be given based on the Debye–Hückel approximation (cf. Hunter [1]) as

$$\rho_e(\bar{y}) \simeq -\frac{q_w}{l_D}\,\mathrm{e}^{-\bar{y}/l_D}. \tag{4}$$

Within Eq. (4) $q_w = \epsilon\epsilon_0\zeta/l_D$ is the charge (per unit area) at the wall, $\epsilon\epsilon_0$ is the dielectric constant within the liquid, ζ is the zeta potential, and l_D is the Debye length. It should be noted that the Debye–Hückel approximation strictly holds for small zeta potentials, i.e. if the electrostatic energy of the ions is much smaller than their thermal energy. For large zeta potential, though the precise amplitude and thickness of the EDL are not captured, it yields a qualitatively correct net charge distribution. A detailed discussion on this aspect and an improved model for large zeta potential can be found e.g. in Janssens-Maenhout and Schulenberg [20]. The net charge distribution in Eq. (4) is derived for

a flat wall. For a curved wall, though, the expression remains an excellent approximation as long as the radius of wall curvature r_0 is much larger than the Debye length l_D. Except at sharp corners, $r_0 \gg l_D$ is certainly given for manufactured microchannels. According to the net charge distribution (4), a wall-normal electrical field

$$E_{\bar{y}0} = \frac{q_w}{\epsilon\epsilon_0}\,\mathrm{e}^{-\bar{y}/l_D} \tag{5}$$

is induced, such that the local wall-normal field component can be expressed by a superposition of the self-induced field $E_{\bar{y}0}$ and the externally-applied field $E_{\bar{y}}$. To non-dimensionalize the above Eqs. (1)–(3) we introduce homogeneous (channel) length scales, a transport time scale, (channel) velocity scales, and a viscous pressure scale, namely

$$(X, Y) = \frac{(\bar{x}, \bar{y})}{d_0}, \quad \tau = \frac{t}{(d_0/u_0)}, \quad (U, V) = \frac{(\bar{u}, \bar{v})}{u_0}, \quad P = \frac{p}{(\mu u_0/d_0)}. \tag{6}$$

Within the scaling (6) d_0 denotes the channel width and u_0 the average axial velocity in the channel. We obtain the dimensionless version of the conservation equations in tangential/normal wall coordinates (X, Y) as

$$\frac{\partial U}{\partial X} + \frac{\partial V}{\partial Y} = 0, \tag{7}$$

$$Re\left(\frac{\partial U}{\partial \tau} + U\frac{\partial U}{\partial X} + V\frac{\partial U}{\partial Y}\right) \simeq -\frac{\partial P}{\partial X} + \frac{\partial^2 U}{\partial X^2} + \frac{\partial^2 U}{\partial Y^2} - \delta^{-2}\Pi_{\bar{x}}\,\mathrm{e}^{-Y/\delta}, \tag{8}$$

$$Re\left(\frac{\partial V}{\partial \tau} + U\frac{\partial V}{\partial X} + V\frac{\partial V}{\partial Y}\right) \simeq -\frac{\partial P}{\partial Y} + \frac{\partial^2 V}{\partial X^2} + \frac{\partial^2 V}{\partial Y^2} - \delta^{-2}\Pi_0\,\mathrm{e}^{-2Y/\delta} - \delta^{-2}\Pi_{\bar{y}}\,\mathrm{e}^{-Y/\delta}. \tag{9}$$

Within Eqs. (7)–(9) the dimensionless groups are defined by

$$Re = \frac{u_0 d_0}{\nu}, \quad \Pi_0 = \frac{q_w^2 l_D}{\epsilon\epsilon_0\mu u_0} > 0, \quad \delta = \frac{l_D}{d_0} \ll 1, \quad \begin{pmatrix}\Pi_{\bar{x}}\\ \Pi_{\bar{y}}\end{pmatrix} = \frac{q_w l_D}{\mu u_0}\begin{pmatrix}E_{\bar{x}}\\ E_{\bar{y}}\end{pmatrix}. \tag{10}$$

Obviously, the (channel) Reynolds number Re and the (small) ratio of length scales $\delta \ll 1$ enter the problem. Π_0 measures the strength of the normal electrical field, induced by the charge distribution (4). The vector $\boldsymbol{\Pi} = (\Pi_{\bar{x}}, \Pi_{\bar{y}})$ is the dimensionless form of the externally-applied electrical field $\mathbf{E}$. Thus, Π_0, $\Pi_{\bar{x}}$, $\Pi_{\bar{y}}$ are all ratios of electrical forces and viscous forces.

Within Eqs. (7)–(9) we have neglected the (weak) electrical field induced by the streaming current against the (strong) externally applied field $\mathbf{E}$. Under this assumption, the flow equations and the electrical field equations are coupled in one direction only. Thus, the applied (plane) electrical field can be computed separately from the flow. For an arrangement of liquid and solid between electrodes, the computation of the applied electrical field is straight forward. Given a spatially-dependent dielectric constant $\epsilon(x, y)$, we have to solve Gauss' law

$$\nabla \cdot (\epsilon \nabla \varphi) = \rho_e(x, y) \tag{11}$$

in conjunction with adequate boundary conditions to obtain the (quasisteady) electrical potential $\varphi(x, y)$. At the electrodes Dirichlet boundary conditions are adequate, as a defined potential is imposed; at the outer boundaries of the computational domain Neumann boundary conditions or third-type boundary conditions are typically adequate. The electrical field $\mathbf{E}(x, y)$ is linked to the electrical potential via

$$\mathbf{E} = -\nabla\varphi. \tag{12}$$

The quasisteady treatment of the electrical problem remains a good approximation even for time-dependent boundary conditions at the electrodes as long as moderate frequencies are applied.

The source term on the right side of Eq. (11) disappears within the bulks of liquid and solid, where electrically-neutral conditions prevail. In the electrical double layer (EDL) we have already approximated ρ_e by Eq. (4). In the frame of the present (separate) treatment of the EDL it is consistent to solve, at first, the homogeneous version of Eq. (11) (for $\rho_e = 0$) to obtain the externally-caused part of the electrical field. Secondly, the superposition of the internal electrical field within the EDL (cf. Eq. (5)) accounts for the source term in the net-charged liquid region.

If the dielectric constants of liquid and solid are similar, i.e. if $\epsilon_l \simeq \epsilon_s$ holds, the externally-caused part of the electrical field is approximately constant for liquid and solid (i.e. the channel) arranged between two line electrodes. Under these conditions the detailed computation of the electrical field is not really necessary and the externally-caused part of the electrical field can be idealized spatially-constant.

2.3. Asymptotic treatment of the electrical double layer

From the momentum equations (8), (9) it is obvious that the electrical terms rapidly decay as we move away from the wall. Thus, to treat the problem using a matched-asymptotic approach is natural. Firstly, within the core region an "outer" solution can be obtained from the standard Navier–Stokes equations (without electrical terms) e.g. by means of some numerical method. Secondly, within the wall layer an "inner" approximate solution can be obtained by rescaling the wall-normal coordinate appropriately and by balancing the leading-order terms within the conservation equations. Finally, an approximate overall solution can be inferred by matching and superposition of the "inner" and "outer" solutions. In detail, the rescaling

$$\widetilde{Y} = \frac{Y}{\delta}, \qquad \widetilde{V} = \frac{V}{\delta}, \tag{13}$$

leads to the leading-order equations

$$\frac{\partial U}{\partial X} + \frac{\partial \widetilde{V}}{\partial \widetilde{Y}} = 0, \tag{14}$$

$$0 \simeq \frac{\partial^2 U}{\partial \widetilde{Y}^2} - \Pi_{\tilde{x}}\, \mathrm{e}^{-\widetilde{Y}}, \tag{15}$$

$$0 \simeq -\frac{\partial P}{\partial \widetilde{Y}} + \frac{\partial^2 \widetilde{V}}{\partial \widetilde{Y}^2} - \delta^{-1}\Pi_0\, \mathrm{e}^{-2\widetilde{Y}} - \delta^{-1}\Pi_{\tilde{y}}\, \mathrm{e}^{-\widetilde{Y}}, \tag{16}$$

valid within the wall layer. The momentum equation (15) reflects a dominant balance between tangential electrical forces and viscous forces within the wall layer, while the momentum equation (16) shows normal electrical forces balanced by pressure forces and viscous forces. The appropriate kinematic boundary conditions are

$$U_w(\tau, X, 0) = 0, \qquad \widetilde{V}_w(\tau, X, 0) = 0. \tag{17}$$

This set of conservation equations and boundary conditions (14)–(17) allows for a leading-order analytical solution for the wall layer (subscript w), namely

$$U_w\big(X, \widetilde{Y}\big) \simeq \Pi_{\tilde{x}}\big\{\mathrm{e}^{-\widetilde{Y}} - 1\big\}, \qquad \widetilde{V}_w\big(X, \widetilde{Y}\big) \simeq 0, \tag{18}$$

$$P_w\big(\tau, X, \widetilde{Y}\big) \simeq \frac{1}{2}\delta^{-1}\Pi_0\, \mathrm{e}^{-2\widetilde{Y}} + \delta^{-1}\Pi_{\tilde{y}}\, \mathrm{e}^{-\widetilde{Y}} + C(\tau, X). \tag{19}$$

Finally, we have to match the wall solution (18), (19) to the core solution (subscript c), obtained e.g. numerically from the standard Navier–Stokes equations. We engage the matching conditions proposed by van Dyke [21]. Matching to first order provides the constraints

$$U_c(\tau, X, 0) \simeq -\Pi_{\tilde{x}}, \quad V_c(\tau, X, 0) \simeq 0, \quad C(\tau, X) \simeq P_c(\tau, X, 0). \tag{20}$$

The kinematic conditions in (20) can be interpreted as boundary conditions for the core solution, whereas the pressure condition in (20) provides a boundary condition for the wall solution. It is important to note that any applied tangential electrical field component ($\Pi_{\tilde{x}} \neq 0$) leads to a slip boundary condition for the core solution, while normal field components, self-induced or applied, cause a rapid pressure variation immediately at the wall. The slip boundary condition in (20) is in agreement with the so-called Helmhotz–Smoluchowski slip velocity discussed in the literature (cf. Probstein [3]). With the known solutions in the wall layer and in the core region, we can infer an approximation for the overall solution by means of the superposition

$$U(\tau, X, Y) \simeq U_w\big(X, \widetilde{Y}\big) + U_c(\tau, X, Y) - U_w\big(X, \widetilde{Y} \to \infty\big), \tag{21}$$

$$V(\tau, X, Y) \simeq V_c(\tau, X, Y), \tag{22}$$

$$P(\tau, X, Y) \simeq P_w\big(\tau, X, \widetilde{Y}\big) + P_c(\tau, X, Y) - P_w\big(X, \widetilde{Y} \to \infty\big). \tag{23}$$

We have tested this matched asymptotic approach for the case of a developed flow between two plates, for which an analytical solution exists. The details are discussed in Appendix A.

3. Principle of an electrically-excited micromixer

We intend to apply electrical forces to improve mixing. The effect of electrical forces can be understood e.g. from simulations of the flow around a cylinder, as given in Fig. 2. The steady flow without electrical forces at a cylinder Reynolds number of $Re_d = u_0 d/\nu = 10$ would be from left to right around the cylinder (not given), involving a steady wake on the right (leeward) side of the cylinder. The result from an applied stationary vertical electrical field are e.g. for $\Pi_x > 0$ stationary forces acting upwards on the liquid in the EDL. At both sides of the cylinder upward streams of higher velocity are obvious in Fig. 2, both from the streamlines and the profile of the vertical velocity. The profile of the vertical velocity, from superposition of core and wall solutions, is given in Fig. 2 as a solid line, while the core solution profile is given for comparison as a dashed line. The liquid leaving the cylinder in the upward direction penetrates into the parallel main flow, which is from left to right. The electrically-induced flow, thus, moves both stagnation points to the positions visible in Fig. 2. If we further oscillate the amplitude of the electrical field, while maintaining its vertical direction, we obtain streams of liquid leaving the cylinder periodically upwards and downwards in time. This periodic distortion of the parallel main flow by penetrating streams can be used to improve mixing, if two miscible liquids flow from left to right, below and above the horizontal symmetry line of the cylinder (cf. Fig. 3(a)). The restriction to miscible liquids arises due to the possibility of an additional EDL at the liquid/liquid interface, which would need appropriate modelling. The mechanism, outlined above, is not limited to cylindrical obstacles within the flow. Whenever walls permit electrically-driven liquid streams into the main flow, this mechanism will likewise work. Thus, other configurations with other obstacle shapes or folded meander channels (cf. Fig. 3(b)) may also lead to improve mixing.

In a generic mixer design two liquids enter the mixer via two supply channels. Both liquids merge into a single channel, where mixing occurs. Through a common channel the mixture leaves the device. We test two different designs of the mixing section. Firstly, a cylindrical obstacle is installed within the mixing section (cf. Fig. 3(a)).

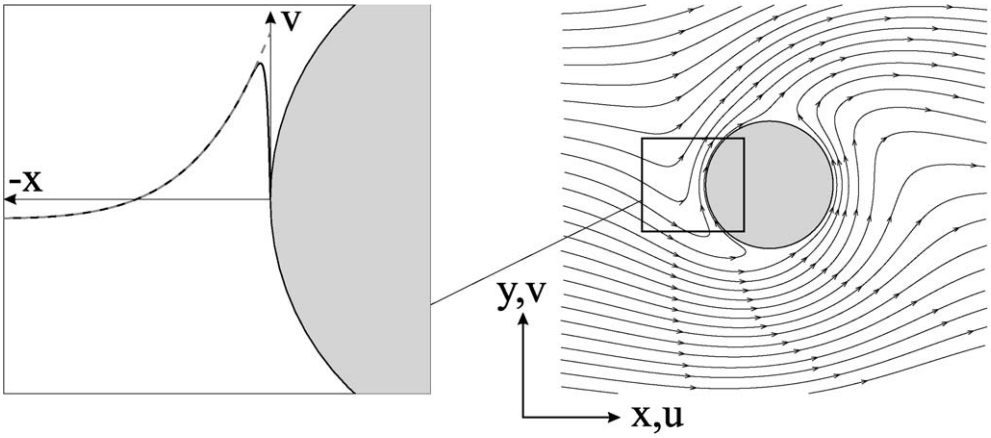

Fig. 2. Steady flow field around a cylindrical obstacle in presence of a stationary vertical electrical field. Parameters are $Re_d = 10$, $\Pi_x = 0$, $\Pi_y = 3$, $\delta = 4 \times 10^{-4}$. The main flow is from left to right.

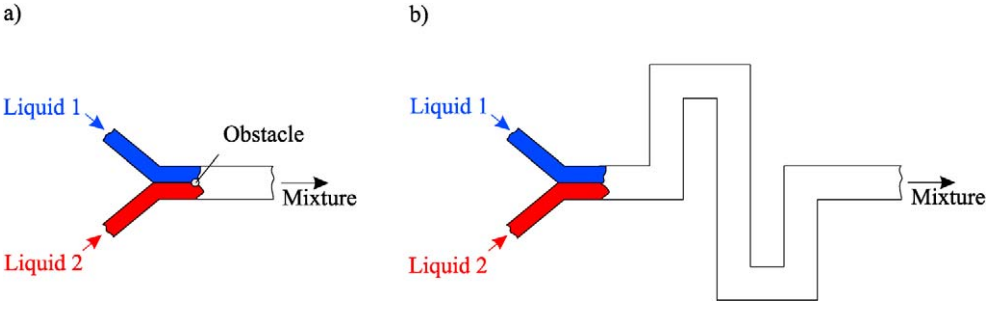

Fig. 3. Principle designs of mixers.

EDLs are present both around the obstacle and at the channel walls. A vertical oscillating electrical field is applied to electrically drive streams perpendicularly into the main flow around the obstacle. Due to this mechanism, the virtual interface between the liquids is stretched, folded and significantly increased to allow for more effective molecular diffusion. Within the EDLs at the channel walls, the vertical electrical field does not cause movement of the liquid, instead periodic pressure oscillations are expected (cf. Eqs. (18), (19)). Secondly, the mixing section is folded to form a meander, as shown in Fig. 3(b). A vertical oscillating electrical field is applied, resulting in electrical forces within the EDLs at the vertical channels walls. As the liquid streams along these walls arrive at corners, they overshoot and penetrate into the main flow. Thus, again the mixing of the two liquids can be enhanced.

4. Simulation results

We engage two-dimensional and time-dependent finite-element simulations for the core solution to investigate the flow fields in the two micromixer designs given in Fig. 3, with and without electrical excitation. All properties of both liquids are assumed to be identical. For the spatial discretization we engage 9-node quadrilateral elements, featuring biquadratic basis functions, which prove to be second-order accurate. For the time stepping an implicit second-order predictor/corrector scheme (explicit Adams–Bashford, stable trapezoidal) is used. Element size and time step are chosen such that at all time steps the solution has converged, so that the RMS of the residuum, summed over all equations, remains smaller than 1×10^{-4}. Particle paths are integrated by a fourth-order Runge–Kutta integration scheme, based on biquadratic interpolation of the velocity field. We employ different means to evaluate the flow and the mixing efficiency: (i) instantaneous streamlines, (ii) dye particles continuously introduced into the flow at fixed positions, and (iii) marker particles positioned at the virtual interface of the liquids to be mixed. The dimensionless parameters for the following simulations, namely Re_d, Re, $\widehat{\Pi}$, F, are chosen such that the velocity amplitude of the excited secondary flow is comparable to the velocity of the forced flow. This allows for a demonstration of the basic treatment and principle of such electroosmotic mixers. We avoid the numerical solution of the mass transport equation and, thus, the computation of the concentration field. In view of the small mass diffusivity D typical for e.g. aqueous solutions, we expect Schmidt numbers $Sc \sim 100$–1000. Simulations with such large Schmidt numbers usually suffer from numerical diffusion and require an enormous computational effort, without providing great additional insight.

4.1. Mixing due to a cylindrical obstacle

A single circular cylinder is positioned as an obstacle in the microchannel, as sketched in Fig. 3(a). The ratio of channel width d_0 and cylinder diameter d is $d_0/d = 14$. The cylinder Reynolds number $Re_d = 10$ is clearly below the critical Reynolds number for the onset of a (naturally-excited) Karman vortex street. Thus, all time-dependent flow phenomena are due to the external electrical excitation. We apply a vertical oscillating electrical field, given by

$$\begin{pmatrix} \Pi_x \\ \Pi_y \end{pmatrix} = \begin{pmatrix} 0 \\ \widehat{\Pi} \sin(2\pi f t) \end{pmatrix}. \tag{24}$$

Its amplitude is $\widehat{\Pi} = 15$ and its non-dimensional excitation frequency is $F = f d_0/u_0$. As a consequence of the applied field, we find along the cylinder contour time-periodic electroosmotic liquid motion where a wall-tangential component of the electrical field is present. The upper and lower channel walls, in contrast, do not exhibit electroosmotic liquid motion, as no wall-tangential electrical field component is present. This can be inferred from the matching conditions (20), which give $U_c(\tau, X, 0) = V_c(\tau, X, 0) = 0$ at all walls, parallel to the X-axis. At the left boundary of the computational domain we have a parallel inflow with $u = u_0$, $v = 0$. At the right boundary of the computational domain we employ a convective outflow condition, namely

$$\frac{\partial u}{\partial t} + u_0 \frac{\partial u}{\partial x} = 0, \qquad \frac{\partial v}{\partial t} + u_0 \frac{\partial v}{\partial x} = 0. \tag{25}$$

The outflow condition (25), as e.g. used by Mück et al. [22], allows periodic vortices to exit the computational domain with very little distortion of the upstream flow field and without pressure oscillations, reflected into the upstream direction.

In Fig. 4 we give a set of instantaneous streamlines, obtained during one period $T = 1/F$ of the sinusoidal excitation. We clearly recognize the oscillating vertical velocity component, introduced at the cylinder. This oscillation is

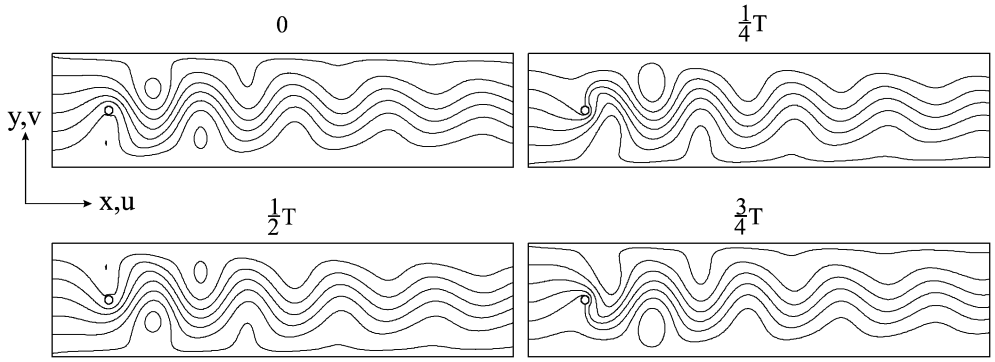

Fig. 4. Instantaneous streamlines for the flow around a cylindrical obstacle in the mixing channel, given in equal time steps for one period T of excitation. The excitation frequency is $F = 1.4$.

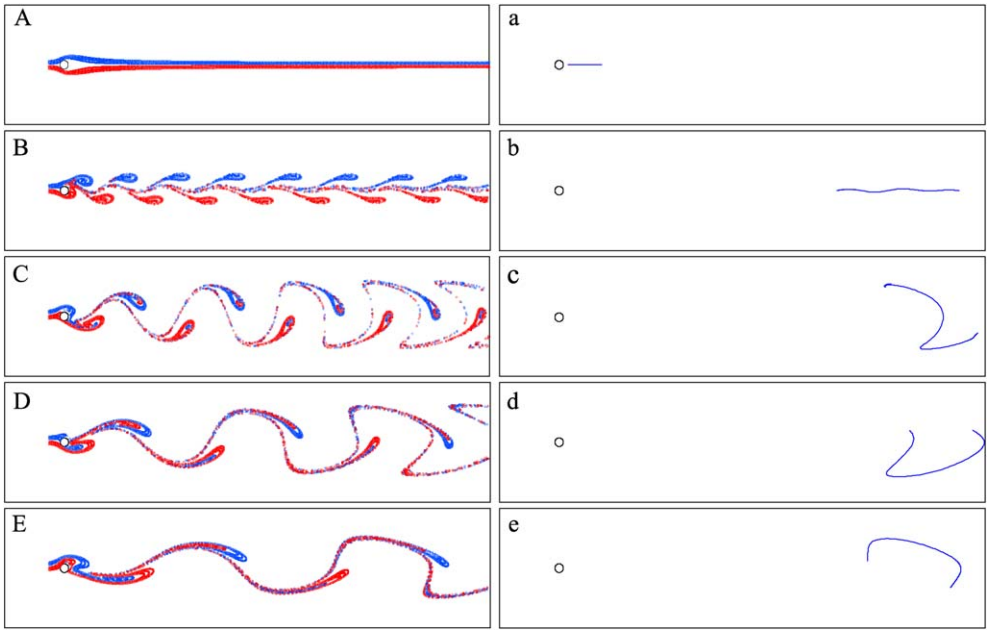

Fig. 5. Particle streak lines and marked virtual interfaces for the flow around a cylindrical obstacle in the mixing channel. Case (A) is obtained without electrical excitation. Case (a) gives the initial marked interface. Cases (B)–(E), (b)–(e) are obtained for excitation frequencies of $F_B = 2.33$, $F_C = 1.4$, $F_D = 0.93$ and $F_E = 0.7$.

swept downstream and damped. The flow field induced by the vertical electrical excitation has some similarity to the flow field induced by a vertically-oscillating cylinder. In both cases near the cylinder contour an oscillating velocity is imposed. While for the oscillating cylinder this appears due to the kinematic boundary conditions on the complete contour, for electrical excitation oscillatory velocities are induced only along parts of the contour, which are parallel to the (vertical) electrical field vector. In order to evaluate the improvement of mixing due to the electrical excitation, it is reasonable to introduce (passive) dye particles into both liquids above (blue) and below (red) the symmetry line. These dye particles have no mass and follow the flow perfectly without slip. By continuously feeding such dye particles into the flow at fixed positions upstream of the cylinder, we obtain information on the behavior of the virtual interface between both liquids. This virtual interface is located where both colours meet. The results for various excitation frequencies F are given in Figs. 5(B)–(E), while for comparison Fig. 5(A) gives the flow without electrical excitation. Without excitation (cf. Fig. 5(A)) the flow is steady, features a steady wake, and the virtual interface between the liquids is straight. In contrast, with excitation (cf. Figs. 5(B)–(E)) the unsteady complex secondary flow stretches and

folds the virtual interface between both liquids repeatedly. Given this larger virtual interface, molecular diffusion can act more effectively and mixing will be enhanced.

The effect of the excitation frequency can be likewise inspected in Figs. 5(B)–(E). For fast oscillation of the electrical field, Fig. 5(B) demonstrates that the virtual interface is only slightly deflected from a straight shape and its length barely increases. As a result the two liquid layers remain largely separated and hardly interact. For slow oscillation of the electrical field (cf. Fig. 5(E)) both liquid layers interact more strongly, leading to portions of one liquid completely surrounded by the other liquid. Thus, the virtual interface appears larger. Due to the low excitation frequency, the number of foldings of the virtual interface (per unit channel length) remains low. By comparing the particle pattern in Fig. 5(E) with the particle patterns in Figs. 5(C), (D) at higher excitation frequencies, the eye already recognizes an optimal excitation frequency, where the virtual interface is maximized. A quantitative measure for the actual length of the virtual interface can be obtained by tracking a row of particles, placed initially onto the virtual interface just behind the cylinder (cf. Fig. 5(a)). As time evolves, these particles are swept downstream by the oscillating flow, such that the initially straight line of particles is stretched and folded. After a certain period of time, this line of particles is given in Figs. 5(b)–(e) for various excitation frequencies. We clearly recognize different lengths and shapes. The increase of the length of this line of particles is linked to the increase of the virtual interface and hence, to the increase of diffusion between both liquids. The lengths for the cases (b)–(e) can be easily computed, while the initial length l_a is given in Fig. 5(a). The ratios of final and initial length are obtained as $l_b/l_a = 4.26$, $l_c/l_a = 5.62$, $l_d/l_a = 5.56$, and $l_e/l_a = 4.41$. This supports the expectation of an optimal excitation frequency, which appears to be between cases (b) and (d), with an excitation frequency of about $F \simeq 1.4$. It should be noted here that this optimal excitation frequency $F = f d_0/u_0 \sim 1$ is associated with the pure channel flow (channel width d_0) and not with the frequency of vortex shedding behind the cylinder (diameter d). This can be concluded firstly from the "natural" frequency u_0/d_0 of the channel flow. Secondly, a comparison to laminar vortex shedding frequencies, summarized for circular cylinders in the range $Re_d \geqslant 40$ by Williamson [23], indicates much smaller frequencies if extrapolated into the stable range towards $Re_d = 10$. The extrapolation, though, remains uncertain. The optimal excitation frequency proves to be independent of the electrical field amplitude.

4.2. Mixing due to a folded (meander) channel

Certainly, the fabrication of a single microcylinder within a microchannel is a non-trivial task. Hence, such a mixer remains purely of academic interest. Therefore, it is reasonable to discuss other geometries, which on the one hand allow for electrical excitation and on the other hand are more easily fabricated. One example is a folded (meander) channel, as given in Fig. 3(b). The parameters chosen to demonstrate the mixing in such a meander channel are $Re = 10$, $\widehat{\Pi} = 6$, $F = 1.4$. For the system water/glass the wall charge is estimated to be $q_w = 5 \times 10^{-3}$ C/m^2, the Debye length to be $l_D \simeq 50$ nm, and the self-induced electrical field results to be $E_{y0} \simeq 7100$ V/mm. The dimensional parameters corresponding to these dimensionless groups are summarized in Table 1. The parameter combination with $Re = 10$ certainly is not typical for lab-on-chip situations. Instead, it is at the limit with regard to Reynolds numbers, which still allow for the electrical excitation of a sufficiently-strong secondary flow. It should be clear, however, that small Reynolds numbers (weak forced flow) require weak secondary flows, and therefore weak electrical fields. We therefore list another set of parameters with $Re = 0.1$ in Table 1, which proves to achieve similar mixing results at lower electrical field strength, according to our simulations. These results will not be discussed in detail. Furthermore, a scaling discussion can be found in Section 5.

At a channel Reynolds number $Re = d_0 u_0/\nu = 10$, the flow without electrical excitation remains steady and laminar, as obvious in Fig. 6. Further, we recognize small steady recirculation regions in all corners. The boundary conditions at the left and right boundary of the computational domain ensure parallel inflow and convective outflow, identical with the boundary conditions employed for the cylindrical obstacle (cf. Section 4.1). A flow as given in Fig. 6

Table 1
Sets of parameters for the folded (meander) channel

Re	u_0 [mm/s]	d_0 [μm]	$\widehat{\Pi}$	$\widehat{E}_y$ [V/mm]
10	50	200	6	1200
0.1	1	100	3	12

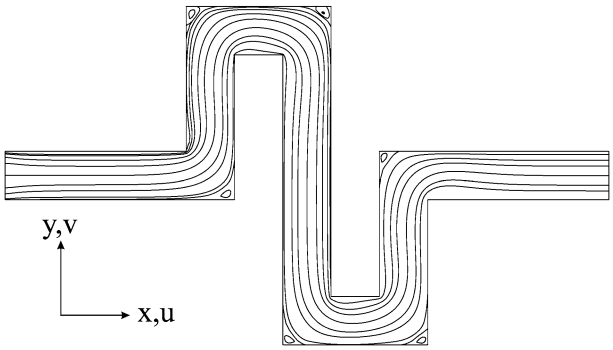

Fig. 6. Streamlines for the steady flow in a folded (meander) channel at $Re = 10$ without electrical excitation.

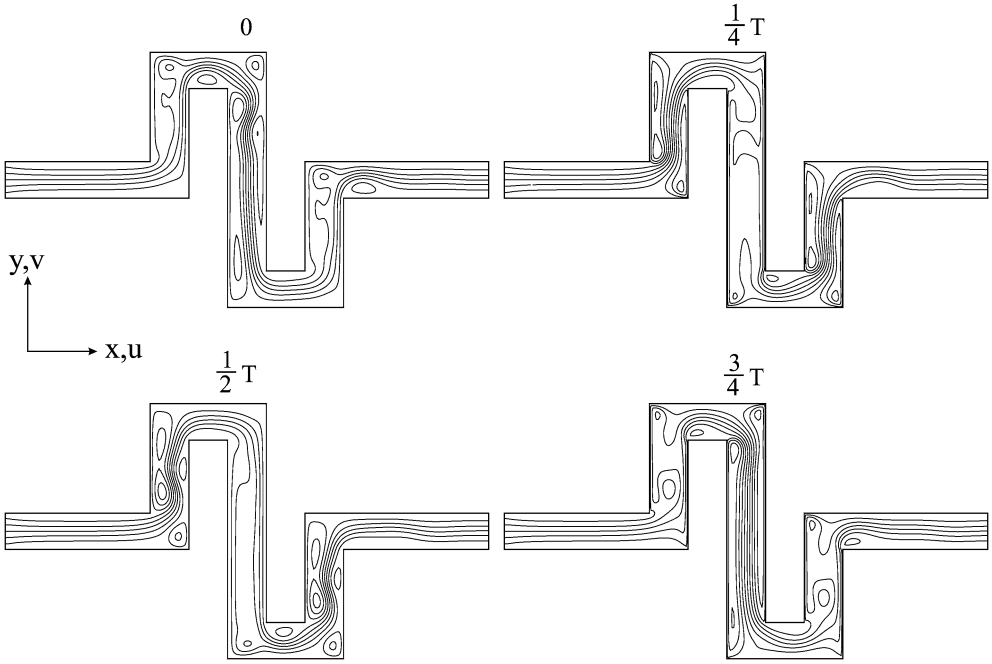

Fig. 7. Instantaneous streamlines for the unsteady flow in a folded (meander) mixing channel, given in equal time steps for one period T of excitation. The (channel) Reynolds number is $Re = 10$, the excitation frequency is $F = 1.4$, the excitation amplitudes is $\widehat{\Pi} = 6$.

will obviously not provide efficient mixing, as the virtual interface between the two liquids remains relatively small, allowing for little molecular diffusion.

If we apply a vertical oscillating electrical field, as given by Eq. (24) with $\widehat{\Pi} = 6$ and $F = 1.4$, we accelerate periodically the liquid along vertical walls. This is a consequence of the matching conditions (20). At walls parallel to the X-axis, in contrast, the matching conditions (20) give $U_c(\tau, X, 0) = V_c(\tau, X, 0) = 0$. The resulting flow is given in Fig. 7 in form of the stream function during one period of excitation. We clearly recognize the strong disturbance of the steady forced flow by time-periodic secondary motion, induced along vertical walls. The effect of the secondary flow on mixing can be inspected in Fig. 8. We again introduce continuously (passive) dye particles at fixed positions into both liquids above (blue) and below (red) the mid axis of the channel. Fig. 8(a) gives the particle distribution without electrical excitation after a certain time. We recognize the virtual interface, roughly along the channel mid where both colours meet. In contrast, with electrical excitation the secondary flow mixes the dye particles, essentially hiding the position of virtual interface. This indicates a strong folding and stretching of the virtual interface, which will allow for more effective subsequent molecular diffusion between both liquids.

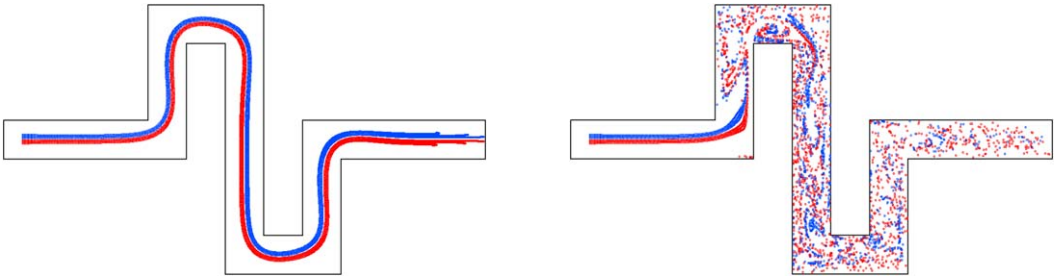

Fig. 8. Particle streak lines for (a) the steady flow without electrical excitation and (b) the time-dependent flow due to electrical excitation. The (channel) Reynolds number is $Re = 10$ in both cases, the excitation frequency for (b) is $F = 1.4$, the excitation amplitudes is $\widehat{\Pi} = 6$.

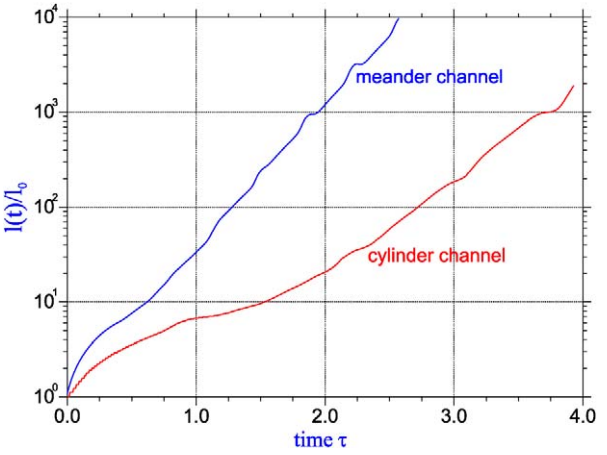

Fig. 9. Area (length) of the virtual interfaces in time, for both the channel with a cylinder ($Re = 10$, $\widehat{\Pi} = 6$, $F = 1.4$) and the folded (meander) channel ($Re = 10$, $\widehat{\Pi} = 6$, $F = 1.4$).

Completely analogously to Section 4.1 (cf. Fig. 5), we can likewise for the folded (meander) channel add a row of particles to track the virtual interface in time. The result for the folded (meander) channel is compared in Fig. 9 against the result for the channel with the cylinder. We recognize in the half-logarithmic diagram, after an initial transient, a roughly-linear behavior for both cases. This indicates exponential growth of the virtual interface in time. The different slopes of the curves in Fig. 9 are due to different constants within the exponential functions. This is not surprising in view of different geometries and different electrical excitation amplitudes $\widehat{\Pi}$. Although we certainly observe exponential growth within the initial time interval $0 \leqslant \tau \leqslant 4$ for both cases, we cannot expect this exponential growth to persist for large distance downstream of both excitation sites. Hence, e.g. for Poiseuille-type flows a power-law growth may result for large times.

5. Summary and outlook

In the present paper we propose a method for efficient mixing of liquids in microchannels. The basic idea is to excite a time-dependent secondary flow within the mixing channel by applying an external oscillatory electrical field. The excitation is induced within the electrical double layers (EDLs), typically present at liquid/solid interfaces if charges (ions) are present within the liquid and if the solid is electrically non-conducting. Two arrangements, namely (i) a cylindrical obstacle within the channel and (ii) a folded (meander) channel, are investigated with regard to their potential to set up a favorable secondary flow. We engage numerical (FEM) simulations to compute the time-dependent flow in the channel core. Within these numerical simulations electrical forces within the EDL can be ignored. Instead, a matched asymptotic method is used to infer an analytical solution for the wall layer. The matching of the wall solution and the numerical core solution provides modified boundary conditions for both regions, and the superposition of the solutions in both regions allows for an approximate overall solution, valid in the entire domain.

The simulations demonstrate the potential of this method. We find for both arrangements that mixing is improved due to an enlargement and folding of the virtual interface between the liquids. Thus, diffusion can act more efficiently. Further, the virtual interface between the liquids can be maximized in area by choosing an optimal excitation frequency. The latter finding implies that excitation in resonance with the eigenfrequency of the flow appears to be one promising means for optimization. As advection transforms temporal frequencies into spatial modes, we can expect that excitation in spatial resonance is a further means for optimal performance. Excitation in spatial resonance would require e.g. further obstacles in appropriate distances downstream of the first obstacle. Similarly, the distance of multiple foldings within a meander should allow to take advantage of spatial resonance.

The above simulations are, of course, a first approximation for the treatment of electrically-excited micromixer flows. The simulations are simplified in various respects. Certainly, flows in roughly square microchannels will be three-dimensional. Two additional walls will be present in three-dimensional simulations, which are both parallel to the electrical field vector. Thus, a time-periodic electroosmotic motion along these walls, in phase with the discussed secondary flows, can be expected. This will transform the two-dimensional secondary flows of our above simulations into three-dimensional secondary flows. Moreover, as discussed by Yi and Bau [24], bends, as present in the meander channel, induce three-dimensional secondary flows with amplitudes increasing with Reynolds number. At some stage, three-dimensional simulations are needed to clarify whether these effects augment the mixing or not. Simulations with two liquids of different properties, including inter-liquid diffusion, are certainly necessary to get more insight into the role of non-symmetric electrical effects and into the role of mass diffusion.

We have neglected the effect of the streaming electrical current against the (strong) applied electrical field. Likewise, we have in parts employed approximations for the electrical field, instead of precise computations of the field within the geometrically-complex arrangement of solid and liquid between two electrodes. Both simplifications certainly will not modify the qualitative effects caused by the oscillating electrical field. However, a more detailed modelling of the electrical field appears necessary if a quantitative comparison with validation experiments is envisioned. Such experiments with water in microchannels and electrical excitation in both configurations (obstacle, meander) are presently in progress at our institute at the Forschungszentrum Karlsruhe.

In general, the mixing process will be effective as long as the velocity amplitude of the excited secondary flow is comparable to the velocity of the forced flow. The forced flow velocity scales as $u_0 \propto Re$ and the velocity amplitude of the secondary flow scales as $\hat{u}/u_0 \propto \widehat{\Pi}$. Thus, $\hat{u}/u_0$ remains constant if $\widehat{\Pi} \propto \widehat{E}_y/u_0$ is kept constant. This means that any reduction of the forced flow u_0 leads to a reduction of the electrical field strength $\widehat{E}_y$, required to excite a comparable secondary flow (of identical $\hat{u}/u_0$). In contrast, due to limitations on the electrical field strength achievable in realistic microdevices, there is an upper limit on u_0, and hence on Re, beyond which a comparable secondary flow cannot be excited. In summary, this method of electroosmotic mixing is limited to moderate and small Reynolds numbers. The above arguments clarify that inertia is not really needed for this electroosmotic mixing.

Appendix A. Validation of the treatment of the EDL

The asymptotic approach can be checked for a fully-developed planar channel flow with an applied electrical field **E**. On one hand for this situation Eqs. (7)–(9) admit the analytical solution

$$U(Y) = \frac{P_0}{2L}\left(\frac{1}{4} - Y^2\right) + 2\Pi_x \,\mathrm{e}^{-1/2\delta}\big[\cosh(Y/\delta) - \cosh(1/2\delta)\big], \tag{A.1}$$

$$V = 0, \tag{A.2}$$

$$P(X,Y) = \frac{P_0}{L}(L - X) + \delta^{-1}\Pi_0 \,\mathrm{e}^{-1/\delta}\cosh(2Y/\delta) - 2\delta^{-1}\Pi_y \,\mathrm{e}^{-1/2\delta}\sinh(Y/\delta). \tag{A.3}$$

For the solution (A.1)–(A.3) we have enforced the no-slip boundary condition at both channel walls and have applied the constant pressure gradient $\partial P/\partial X = -P_0/L$. L is the length of the channel along which the pressure difference P_0 is applied. On the other hand we can infer analytically the wall solutions for both walls and can superimpose these solutions onto the core solution, which in this case is simply the pressure-driven Poiseuille flow between the plates. The superimposed profiles $U(Y)$ from the asymptotic approach are plotted in Fig. A.1(a) for $\delta = 0.01, 0.03$ and for an applied tangential electrical field $2\Pi_x L/P_0 = 0.1$. The core solution is likewise given in Fig. A.1(a), as a dotted line, for comparison. The electrical field Π_x introduces forces within the EDL, which in this case ($\partial P/\partial X < 0$, $\Pi_x > 0$)

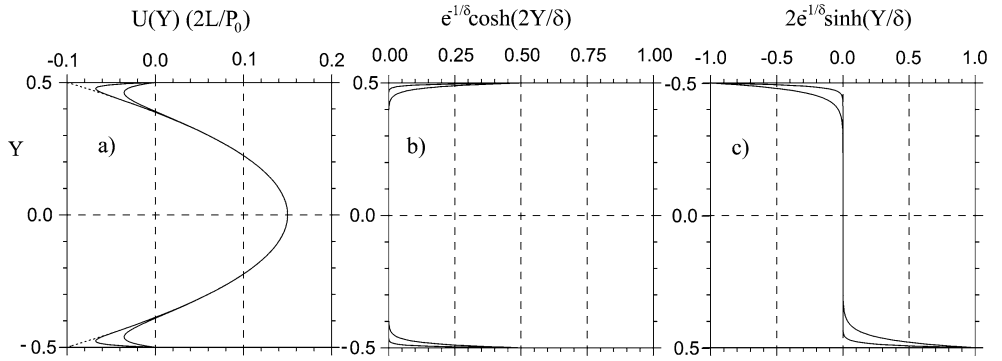

Fig. A.1. (a) Tangential velocity profiles, (b) pressure modification due to self-induced electrical field Π_0, (c) pressure modification due to external normal electrical field $\Pi_y > 0$, all for the developed flow between two parallel plates.

act tangentially against the pressure-driven flow. In the EDL we recognize wall streams directed to the left, while in the core a parabolic profile with flow to the right is present. With decreasing δ we find decreasing thickness of the wall streams. Further, with decreasing δ the amplitude of the wall streams increases until the core solution (dotted line) is approached in the limit $\delta \to 0$. For this particular situation of a developed flow, the superimposed asymptotic solution proves to be identical with the exact solution (A.1)–(A.3). This is true because nonlinear convective terms are absent within the conservation equations for developed flows. The pressure field (A.3) indicates that the self-induced electrical field always causes an increase of pressure in the wall layers at both walls, due to $\Pi_0 > 0$ at all times. This contribution is shown in Fig. A.1(b) for $\delta = 0.01, 0.03$. This pressure increase in the wall layer does not lead to any (unphysical) net force onto the wall, since this pressure force is always balanced by an electrical force of opposite direction due to the charged wall. The applied wall-normal field Π_y causes both a pressure increase and a pressure decrease within the wall layers at opposite walls. This contribution e.g. for the case $\Pi_y > 0$ is plotted in Fig. A.1(c) for $\delta = 0.01, 0.03$.

References

[1] R.J. Hunter, Zeta Potential in Colloid Science; Principles and Aplications, Academic Press, London, 1981.
[2] A.W. Adamson, A.P. Gast, Physical Chemistry of Surfaces, Wiley, New York, 1997.
[3] R.F. Probstein, Physicochemical Hydrodynamics, Wiley, New York, 1994.
[4] M. Gad-el-Hak, The fluid mechanics of microdevices, J. Fluids Engrg. 121 (1999) 5–33.
[5] D. Burgreen, F.R. Nakache, Electrokinetic flow in ultrafine capillary slits, J. Phys. Chem. 68 (1964) 1084–1091.
[6] C.L. Rice, R. Whitehead, Electrokinetic flow in a narrow capillary, J. Phys. Chem. 69 (1965) 4017–4024.
[7] N.A. Patankar, H.H. Hu, Numerical simulation of electroosmotic flow, Anal. Chem. 70 (1998) 1870–1881.
[8] M.J. Kim, A. Beskok, K.D. Kihm, Electro-osmosis-driven micro-channel flows: a comparative study of microscopic particle image velocimetry measurements and numerical simulations, Exp. Fluids 33 (2002) 170–180.
[9] S. Ghosal, Lubrication theory for electro-osmotic flow in a microfluidic channel of slowly varying cross-section and wall charge, J. Fluid Mech. 459 (2002) 103–128.
[10] S.C. Jakeway, A.J. de Mello, E.L. Russel, Miniaturized total analysis systems for biological analysis, Fresenius J. Anal. Chem. 366 (2000) 525–539.
[11] J.M. Ottino, The Kinematics of Mixing: Stretching, Chaos, and Transport, Cambridge University Press, Cambridge, 1989.
[12] V. Hessel, S. Hardt, H. Löwe, F. Schönfeld, Laminar mixing in different interdigital micromixers: I. Experimental characterization, AIChE J. 49 (2003) 566–577.
[13] S. Hardt, F. Schönfeld, Laminar mixing in different interdigital micromixers: II. Numerical simulations, AIChE J. 49 (2003) 578–584.
[14] R.H. Liu, A. Stremler, K.V. Sharp, M.G. Olson, J.G. Santiago, R.J. Adrian, H. Aref, D.J. Beebe, Passive mixing in a three-dimensional serpentine microchannel, J. Microelectromech. Systems 9 (2000) 190–197.
[15] D.J. Beebe, R.J. Adrian, M.G. Olson, M.A. Stremler, H. Aref, B.-H. Jo, Passive mixing in microchannels: fabrication and flow experiments, Mec. Ind. 2 (2001) 343–348.
[16] A.D. Stroock, S.K.W. Dertinger, A. Ajdari, I. Mezić, H.A. Stone, G.M. Whitesides, Chaotic mixer for microchannels, Science 295 (2002) 647–651.
[17] M. Yi, S. Qian, H.H. Bau, A magnetohydrodynamic chaotic stirrer, J. Fluid Mech. 468 (2002) 153–177.
[18] S. Qian, H.H. Bau, A chaotic electroosmotic stirrer, Anal. Chem. 74 (2002) 3616–3625.
[19] M.H. Oddy, J.G. Santiago, J.C. Mikkelsen, Electrokinetic instability micromixing, Anal. Chem. 73 (2001) 5822–5832.

[20] G. Janssens-Maenhout, T. Schulenberg, An alternative description of the interfacial energy of a liquid in contact with a solid, J. Colloid Interface Sci. 257 (2003) 141–153.
[21] M. van Dyke, Perturbation Methods in Fluid Mechanics, The Parabolic Press, Stanford, 1975.
[22] B. Mück, C. Günther, U. Müller, L. Bühler, Three-dimensional MHD flows in rectangular ducts with internal obstacles, J. Fluid Mech. 418 (2000) 265–295.
[23] C.H.K. Williamson, Defining a universal and continuous Strouhal–Reynolds number relationship for the laminar vortex shedding of a circular cylinder, Phys. Fluids 31 (1988) 2742–2744.
[24] M. Yi, H.H. Bau, The kinematics of bend-induced mixing in micro-conduits, Int. J. Heat Fluid Flow 24 (2003) 645–656.